Socrates Dokos
e-mail: s.dokos@unsw.edu.au

Ian J. LeGrice
e-mail: i.legrice@auckland.ac.nz

Bruce H. Smaill
e-mail: b.smaill@auckland.ac.nz

Department of Physiology,
School of Medicine,
University of Auckland,
Private Bag 92019,
Auckland, New Zealand

Julia Kar
Department of Engineering Science,
School of Engineering,
University of Auckland,
Auckland, New Zealand
e-mail: jk1@cec.wustl.edu

Alistair A. Young
Department of Physiology,
School of Medicine,
University of Auckland,
Private Bag 92019,
Auckland, New Zealand
e-mail: a.young@auckland.ac.nz

A Triaxial-Measurement Shear-Test Device for Soft Biological Tissues

A novel shear-test device for soft biological tissue, capable of applying simple shear deformations simultaneously in two orthogonal directions while measuring the resulting forces generated in three axes, is described. We validated the device using a synthetic gel, the properties of which were ascertained from independent tensile and rotational shear tests. Material parameters for the gel were fitted using neo-Hookean analytical solutions to the independent test data, and these matched the results from the device. Preliminary results obtained with rat septal myocardium are also presented to demonstrate the feasibility of the apparatus in determining the shear characteristics of living tissue.
[S0148-0731(00)00205-3]

Introduction

The development of realistic computer models of mechanical behavior for soft biological tissues in health and disease is dependent on the formulation of appropriate constitutive laws and accurate identification of their material parameters. In the past, uniaxial or biaxial tensile testing has been widely used to characterize the material behavior of soft tissues [1]. For many tissue types, however, such tests do not represent the normal mode of deformation *in vivo*, or do not yield sufficient quantitative information to formulate a reliable constitutive law. For instance, biaxial tensile tests have previously been carried out on thin sections of noncontracting myocardial tissue removed from the left ventricle of the heart [2,3]. However, such experiments may give rise to artifactual results where the microstructural integrity of the tissue is disrupted by sectioning [4]. Moreover, myocardial tissues undergo complex patterns of tensile, compressive, and shear deformations throughout the cardiac cycle, and it has recently been shown that the shearing of adjacent muscle layers contributes significantly to subendocardial wall thickening during systole [5]. It follows that *in vitro* tests that incorporate shear and/or compressive loading should provide a more complete characterization of the material behavior of myocardium than biaxial tensile tests alone. Other tissues for which shear characterization would be useful include aortic valve cusps, which undergo significant shearing during normal function [6], and tissues such as brain in which large shear strains and rates have been implicated in tissue trauma [7].

In this study, we describe a shear-test device for soft biological tissue capable of applying simple shear deformations simultaneously in two orthogonal directions, while measuring the resulting forces generated in three axes. The system was designed to apply shear in more than one principal direction so that the degree of anisotropy of the test specimen could be directly addressed. By measuring the forces acting in three orthogonal directions, it is possible to set the initial state of compression and fully characterize the imposed loads. Although shear-test devices for biological samples have been developed in the past [6,8,9], none has incorporated these requirements. We validate the device using small samples of a synthetic gel and present preliminary results obtained in myocardial tissue.

Device Specifications

In developing a device for testing biological samples under simple shear deformation, we were influenced by the following considerations:

(i) The ability to impose shear deformation in two orthogonal directions was seen to be necessary for systematic investigation of material anisotropy.
(ii) Forces must be measured in three orthogonal directions, to characterize loading conditions fully.
(iii) The specimen must be immersed in an appropriate physiological bathing solution throughout the testing process.
(iv) The system must be capable of testing small tissue specimens,[1] as well as measure relatively low shear and compressive forces (anticipated to be within ± 500 mN).

Contributed by the Bioengineering Division for publication in the JOURNAL OF BIOMECHANICAL ENGINEERING. Manuscript received by the Bioengineering Division February 24, 1999; revised manuscript received March 28, 2000. Associate Technical Editor: L. J. Soslowsky.

[1]For appropriately sectioned samples of ventricular myocardium, specimen dimensions of $5 \times 5 \times 2$ mm were seen to provide the best compromise between preservation of structural integrity and ensuring that the tissue is relatively uniform throughout the specimen volume.

(v) The system must resolve nonlinear behavior under large deformations (typically 50–100 percent shear strains).

Methods

Overview of Shear-Test Device. The main components of the shear test system we developed are illustrated in Fig. 1. The device consists of separate $X-Y$, and Z translation stages attached to a fixed base. Mounted on the $X-Y$ translation stage are a tissue bath assembly and the pressure transducer used to measure force in the Z direction. A custom-built transducer, designed to allow forces in the X and Y directions to be measured independently, is fixed above the tissue bath. The tissue specimen is positioned between two circular platforms attached to the $X-Y$ force transducer and the tissue bath assembly respectively, and secured to them using a surface adhesive. The vertical position of the specimen can be set to within an accuracy of 0.1 mm using manual controls and a vernier measuring scale attached to the Z translation stage. To carry out a shear test, the bottom surface of the specimen was displaced horizontally using the $X-Y$ translation stage, while associated forces in X, Y, and Z directions were measured.

***X–Y* Displacement.** Two linear DC motors (DC-Mike drives M-224.07 with C121.05 gear heads, Physike Instrumente) were used to drive the $X-Y$ translation stage (M-015, Physike Instrumente). Each motor was equipped with two magnetic encoders, which output square wave signals in quadrature as the motor spindle rotated, enabling displacement to be measured with a resolution of 0.8 μm in a full travel of 25 mm. Maximum velocity of the motors was 2 mm·s^{-1}.

Vertical *Z* Force Measurement. In order to measure the vertical forces acting on the tissue sample, the lower platform on which the tissue rests was coupled to a variable-reluctance, differential pressure transducer (Validyne MP45-1, Engineering Corp.) with a range of ± 0.2 kPa. The lower shear platform (10 mm diameter) was glued to a circular glass cover slip (25 mm diameter, 0.15 mm thickness, Mediglass), which formed the floor of the tissue bath. The cover slip deflected slightly under vertical load, but was sufficiently rigid in the lateral direction to reject horizontal loads in the direction of shear. A chamber immediately below the bath was coupled to one side of the pressure transducer. This assembly was filled with water and sealed using a fine rubber membrane separated from the cover slip by a thin spacer. The tissue bath and transducer were rigidly fixed to the translation stage.

Horizontal *X – Y* Force Measurement. The components of the $X-Y$ force transducer shown in the upper part of Fig. 1 are illustrated in detail in Fig. 2(*a*), which outlines the basic assembly of concentric brass rings, stainless steel beams, and strain gages used to measure the shear forces applied to the tissue. Each of the rings was connected to its neighbor by four stainless steel beams ($30\times5\times0.25$ mm). The upper platform was fixed to the center of the innermost ring. Each beam was able to deflect laterally, but was relatively stiff and inflexible along its other axes. Thus, when force was applied to the tissue platform in the X direction (Fig. 2(*b*)) the inner beams deflected, while application of a force in the Y direction (see Fig. 2(*c*)) deflected the outer beams. Semiconductor strain gages (KSP-2-120-E3, Kyowa Electronic Instruments) were mounted on opposite sides of one inner beam to register the X force component, while a second pair mounted on an outer beam registered the Y force.

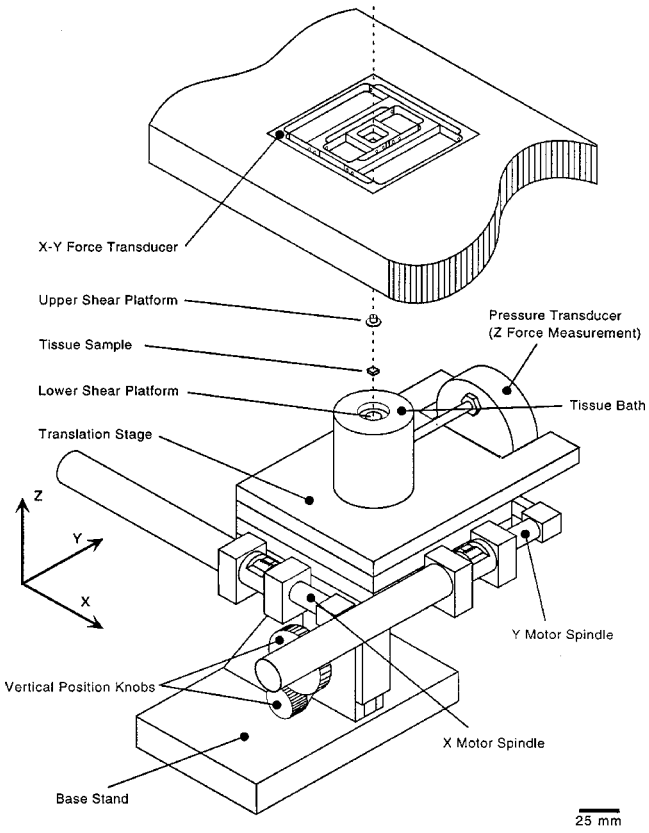

Fig. 1 Schematic overview of Shear-Test Device (drawn to scale). See text for further explanation.

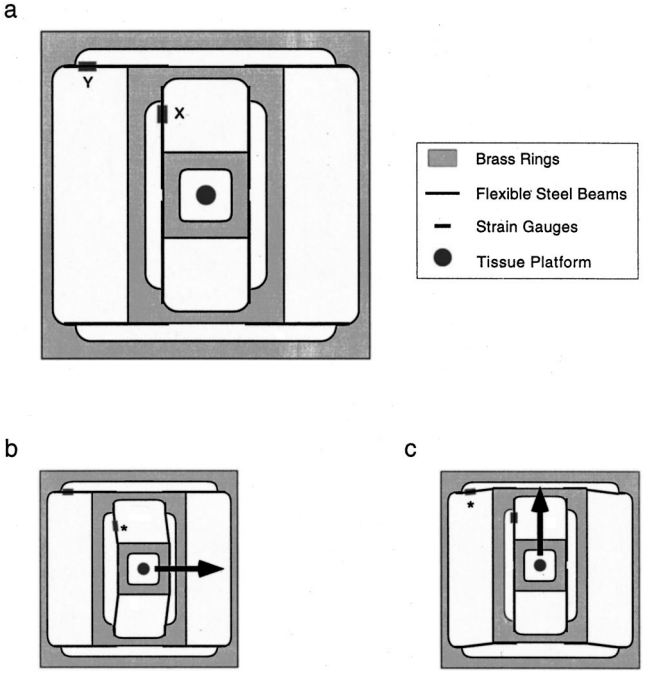

Fig. 2 (*a*) Top view of *X-Y* force transducer used to separate the horizontal *X*, *Y* forces generated on the upper surface of the tissue due to horizontal displacement of its lower surface. A tissue platform that makes contact with top surface of the tissue sample is fixed to the center of the inner ring. (*b*) Displacement of inner ring due to force applied in the *X* direction. The asterisk marks the location of strain gages that separate out and measure this *X* force. (*c*) Displacement of middle and inner rings due to force applied in the *Y* direction. As in (*b*), the asterisk marks the location of strain gages that selectively measure this *Y* force. Note that in diagrams (*b*) and (*c*), the extent of ring deflection is exaggerated for illustrative purposes.

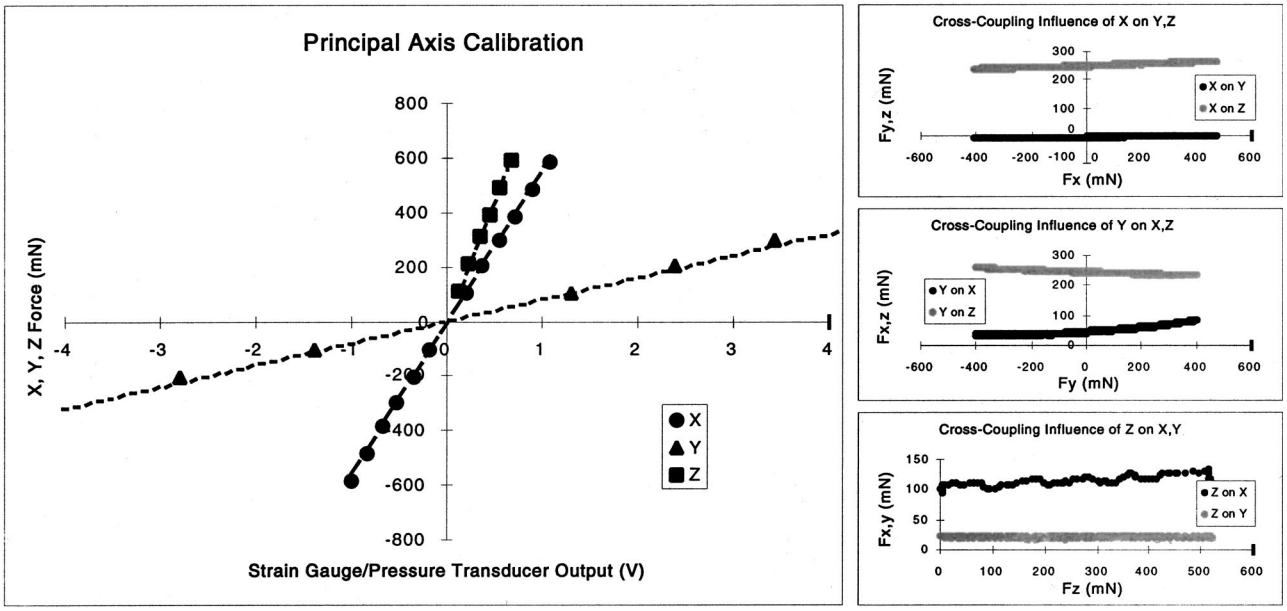

Fig. 3 Typical calibration curves obtained following the protocols described in the text. The principal axis calibrations (left panel) were obtained using the manual calibration procedure outlined in the text. Linear regression fits (dashed lines) were used to determine the principal calibration coefficients comprising the diagonal terms of the 3×3 calibration matrix. Cross-coupling plots (right panels) were then generated by fixing a rigid sample between the upper and lower tissue platforms of the device. The lower platform was then translated in each of the three principal directions separately, with forces recorded and shown in the right panel plots. For these rigid tests, forces were determined using the principal axis coefficients of the preceding manual calibration routine. The rigid tests were a direct way to measure the cross-influences of each principal force on the other two axes. From top to bottom on the right, the panels show the magnitude of cross-talk of an *X* force referred to the *Y* and *Z* directions, a *Y* force referred to *X* and *Z*, and a *Z* force referred to *X* and *Y*. Linear regression fits to these test results were then used to determine the remaining off-diagonal terms of the calibration matrix.

Motor Control and Data Acquisition. The shear testing system was controlled and data were acquired using a Macintosh 9150/120 PowerPC computer equipped with analog interface and timer I/O boards (National Instruments™ NB-M10-16 and NB-TIO-10, respectively). All instrumentation software was written using the LabVIEW (National Instruments™) programming language.

The DC motors were driven independently via the analog interface and quadrature signals from each motor were continuously monitored to provide a real-time measure of displacement. A PID control algorithm was used to impose a variety of programmed shear protocols (sequences of sinusoidal, triangular, or step displacements).

The *X* and *Y* strain gages were interfaced with bridge amplifiers that incorporated low-pass filters (10 Hz, 2 pole). Output from the *Z* pressure transducer was passed through a low-pass filter (1 Hz, 1 pole). These signals were acquired at 60 Hz and converted online to force using a 3×3 calibration matrix generated prior to each test as described below.

Device Calibration. A simple procedure was used to impose forces on the upper tissue platform in order to calibrate the $X-Y$ force transducer. Four long threads aligned in the *X* and *Y* directions were fixed at one end to the upper tissue platform and at the other to a rigid support some 30 cm from the transducer. Weights were suspended from the centers of the threads. The outer attachment points were carefully positioned so that the thread was (*i*) horizontal between the platform and the point at which the weight was suspended and (*ii*) at 45 deg to the horizontal between this point and the outer attachment. This arrangement ensured the vertical force applied by the weight was also imposed in the horizontal direction.

The *Z* pressure transducer was calibrated by placing known weights on the lower tissue platform. A typical calibration plot of all three axes of the device is shown in the left panel of Fig. 3, where the linearity of the device is evident throughout the range of forces tested (±600 mN). Linear regression analysis was used to determine the three principal axis calibration coefficients.

The extent of cross-axis coupling in the shear test device was quantified as follows: A rigid aluminum cuboid (5×5×2 mm) was fixed between the upper and lower tissue platforms and forces on each axis were recorded as the lower platform was translated separately in each of the three principal directions. Plots of cross-axis force versus principal-axis force generated from such a rigid body test are shown in the right-hand panels of Fig. 3. Linear regression analysis was then used to estimate six cross-talk calibration coefficients. These coefficients were negated and incorporated into a 3×3 calibration matrix to convert raw voltages from each of the *X*, *Y*, and *Z* transducers (V_x, V_y, V_z) into units of force (F_x, F_y, F_z) according to

$$\begin{pmatrix} F_x \\ F_y \\ F_z \end{pmatrix} = \begin{pmatrix} C_{xx} & C_{xy} & C_{xz} \\ C_{yx} & C_{yy} & C_{yz} \\ C_{zx} & C_{zy} & C_{zz} \end{pmatrix} \times \begin{pmatrix} V_x \\ V_y \\ V_z \end{pmatrix}$$

where the diagonal terms C_{xx}, C_{yy}, and C_{zz} are the principal calibration coefficients, with the remaining off-diagonal terms serving to null the effects of any axis cross-talk.

The calibration matrix $C_{ij}(\pm \mathrm{SE})$ for the data presented in Fig. 3 was

$$C = \begin{pmatrix} 560.0 \pm 6.1 & -4.7 \pm 0.3 & -43.4 \pm 2.7 \\ -2.3 \pm 0.1 & 80.1 \pm 3.6 & 3.5 \pm 0.3 \\ -18.2 \pm 0.3 & 2.7 \pm 0.1 & 886.3 \pm 12.0 \end{pmatrix} \ \mathrm{mN \cdot V^{-1}}$$

and these are typical values.

Strain Correction. In this device, shear loading is imposed by controlled displacement of the lower tissue platform. However,

measurement of X and Y forces is necessarily associated with small displacements of the upper tissue platform (see Fig. 2). This decreases the relative displacement between platforms, which could cause a slight overestimation of shear strain. The data required to characterize the transducer force displacement relationship are available from the cross-coupling tests described above. For all rigid-body calibrations performed, the force-displacement characteristic was linear. Regression analysis was used to determine two strain correction coefficients a_x, a_y to correct for shear displacement according to

$$s_x = s_x^* - a_x F_x$$

$$s_y = s_y^* - a_y F_y$$

where s_x, s_y are the corrected displacements, s_x^*, s_y^* are the uncorrected displacements determined from the motor positions, and F_x, F_y are the horizontal forces. Strain correction coefficients a_x, a_y were typically 112 and 243 $\mu\text{m}\cdot\text{N}^{-1}$, respectively.

Gel Test Validations. To validate the shear device, tests were carried out on small samples of synthetic silicone gel (Sylgard 527, Dow Corning) whose elastic properties have been shown previously to be similar to soft biological tissue [7]. The material properties of the gel were also characterized with independent tensile tests and rotational shear tests, illustrated schematically in Fig. 4.

The mixed gel components (75 percent resin: 25 percent catalyst) were placed in a sealed chamber and degassed with a vacuum water pump to remove any air bubbles. The mixture was poured into small cuboid moulds ($6\times6\times2$ mm) to provide specimens for the shear test device. The same mixture was poured into long thin cylinders (5.3 mm D) for tensile testing and into an annular cylindrical mould for rotational shear testing. In the latter case, the mould consisted of the annular space (16 mm ID, 38 mm OD, height 24 mm) between concentric plexiglass cylinders. All samples were cured as a single batch for seven hours at 50°C. Using this protocol, two sets of samples were tested from two different batches of gel.

Simple shear tests were carried out with the 6×6 mm surfaces of the cuboid gel specimens fixed to the upper and lower tissue platforms with cyanoacrylate adhesive. Care was taken to ensure that both surfaces of the gel were entirely covered with adhesive, in order to obtain as uniform a strain as possible throughout the sample during testing.

For the tensile tests (Fig. 4(a)), material markers spaced evenly at 2 mm were drawn with a fine pen on the thin cylindrical gel specimen. The specimen was vertically suspended and weights attached to its lower end. Video images were recorded from a central region of the sample to ensure strain uniformity. This was verified by the maintenance under load of regular spacing between material markers in the region of interest. Weights were added in increments of approximately 20 mN until failure of the sample.

For the rotational shear test (Fig. 4(b)), the cylindrical mold and annular gel specimen were mounted so that the outer plexiglas cylinder rested on a thrust-bearing while the inner cylinder was fixed. Thus the outer cylinder was able to rotate under the action of an applied couple while the inner cylinder was not, imposing a rotational shear on the gel in the annular space. Forces were applied via two parallel strings attached horizontally in grooves on the outer cylinder. Material markers consisting of fine silica particles were placed on the upper surface of the sample at various radial distances from the axis of rotation. For each load application, video images were recorded and used to track the angle of rotation of each material point. Results from simple shear, tensile and rotational shear tests were fitted to neo-Hookean analytic solutions (Eqs. (3), (6), and (13) in appendix) using linear and nonlinear least-square procedures.

Tissue Shear Tests. Shear tests were carried out on blocks of myocardium isolated from rat heart septums. Rats weighing around 450 g were anesthetized using halothane, the heart was rapidly excised and perfused retrogradely with cardioplegic solution at 4°C to which 100 mM 2,3-butanedione monoxime (BDM) had been added. BDM is known to block actin–myosin interaction in cardiac muscle and prevents contracture due to cutting injury [10]. The interventricular septum was dissected out and a 5×5 mm square full thickness sample was removed with two edges aligned in the apex–base direction. Immediately following dissection, the thickness of the specimen was measured using a micrometer. The specimen was aligned with the apex–base direction along the x axis and was glued to the lower tissue platform of the shear-test device using a thin coat of cyanoacrylate adhesive. The adhesive was then applied to the upper tissue surface and the bath assembly was raised manually until the specimen contacted the upper tissue platform. A load of 400–600 mN was applied for approximately five minutes to facilitate adhesion of the surfaces. Cardioplegic solution (containing BDM) was then added to the bath and the stage was lowered to zero the compressive force. Following each test (tissue or gel), the sample was removed and carefully examined for evidence of glue penetration, excess glue along free walls, or detachment of the sample from either upper or lower device platforms. If this was the case, results of the test were rejected.

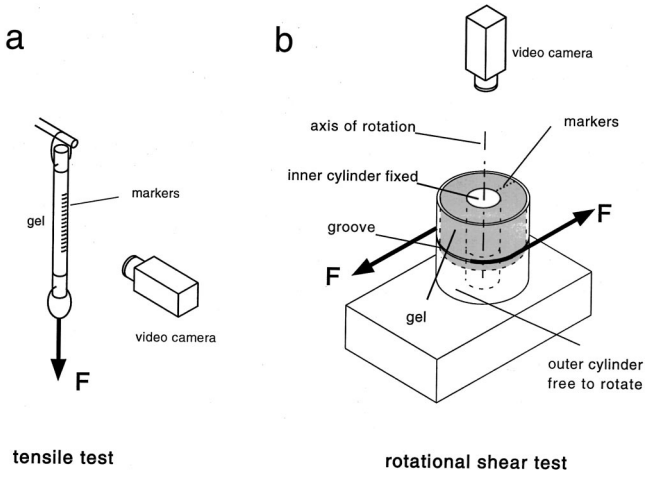

Fig. 4 Test protocols to ascertain independently the material properties of gel samples used to validate the shear test device. In the tensile test (*a*), a thin cylindrical sample of gel (diameter 5.3 mm) was suspended vertically with weights attached to its lower end. A video camera was used to record and measure the distance between evenly spaced material markers to ascertain strain. In the rotational shear test (*b*), a concentric cylindrical sample of gel (outer diameter 38 mm, inner diameter 16 mm, height 24 mm) was cast between two cylindrical tubes and mounted so that the inner cylinder was held stationary while the outer surface was free to rotate under the action of an applied couple. The outer cylinder was supported by a thrust-bearing base to minimize the effects of friction and gravitational load on the sample. Two strings (shown as *F* arrows) attached within grooves on the outer cylinder were used to apply a known couple. Material markers on the top surface of the sample, as recorded by video, were used to measure the angle of rotation of each material point as a function of its radial position in the sample.

Results

Gel Material Properties. To characterize the material properties of the synthetic gel specimens used to validate the shear test device, separate tensile and rotational shear tests were carried out with matched gel samples from two batches. Representative results from one gel batch are shown in Fig. 5. For both batches, a neo-Hookean material description employing a single parameter provided reliable fits to the test data. On the other hand, it was not

possible to identify two unique material parameters reliably using the more complex Mooney–Rivlin characterization [11]. The broken lines in Fig. 5 are best-fit analytic solutions for a neo-Hookean elastic solid in the two different tests (see appendix for derivation of analytic solutions). In both gel batches, the neo-Hookean material parameter identified in the tensile test was 7–10 percent larger than that obtained from the rotational shear test. Results are summarized in Table 1.

Gel Shear Results. Using the shear test device, stress–strain characteristics for the cuboid gel samples under simple shear were obtained for both batches, with representative results from batch 1 shown in Fig. 6. Sinusoidal time-varying shear strains of amplitude 0.25 (0.5 mm displacement) and period 30 s were applied over two cycles in the two *X*, *Y* directions separately. Shear displacements in the *X* direction produced no change in force in the *Y* direction and vice versa (not shown). The stress–strain characteristic was linear, as expected for a neo-Hookean material. For both gel batches, the rotational shear parameter provided the closer fit to the data from the device than that parameter obtained from the tensile tests (see Table 1 and Fig. 6). Reproducibility of the device was examined by testing three separate cuboid samples in succession from batch 2. Variation in C_1 values from the three tests was ± 2 percent of the mean value. Table 1 shows the median value of C_1 obtained from the three samples of batch 2. All shear tests from the device yielded C_1 values that were within 15 percent less than the rotational shear parameter from the corresponding batch of gel.

Myocardial Shear Results. Following validation of the device using the synthetic gel, we examined the shear characteristics of a sample of rat septal tissue. The tissue block measured $5 \times 5 \times 2.2$ mm, with the smallest dimension being the septal thickness. The sample was mounted with left ventricular (LV) and right ventricular (RV) surfaces placed top and bottom, respec-

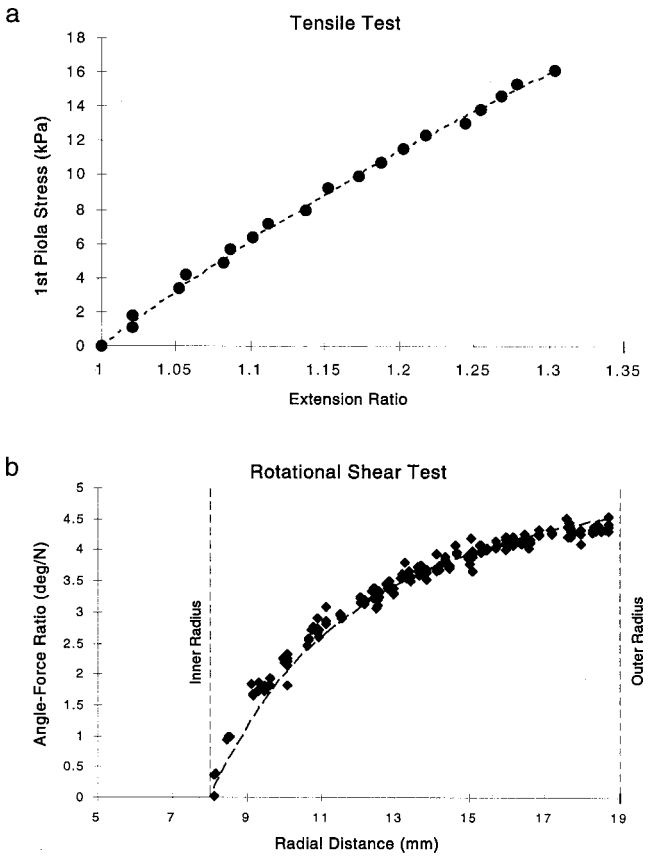

Fig. 5 Gel data from (*a*) tensile and (*b*) rotational shear tests from batch 1 samples. Dashed curve on each graph is the least squares fit of neo-Hookean analytical solution to the data.

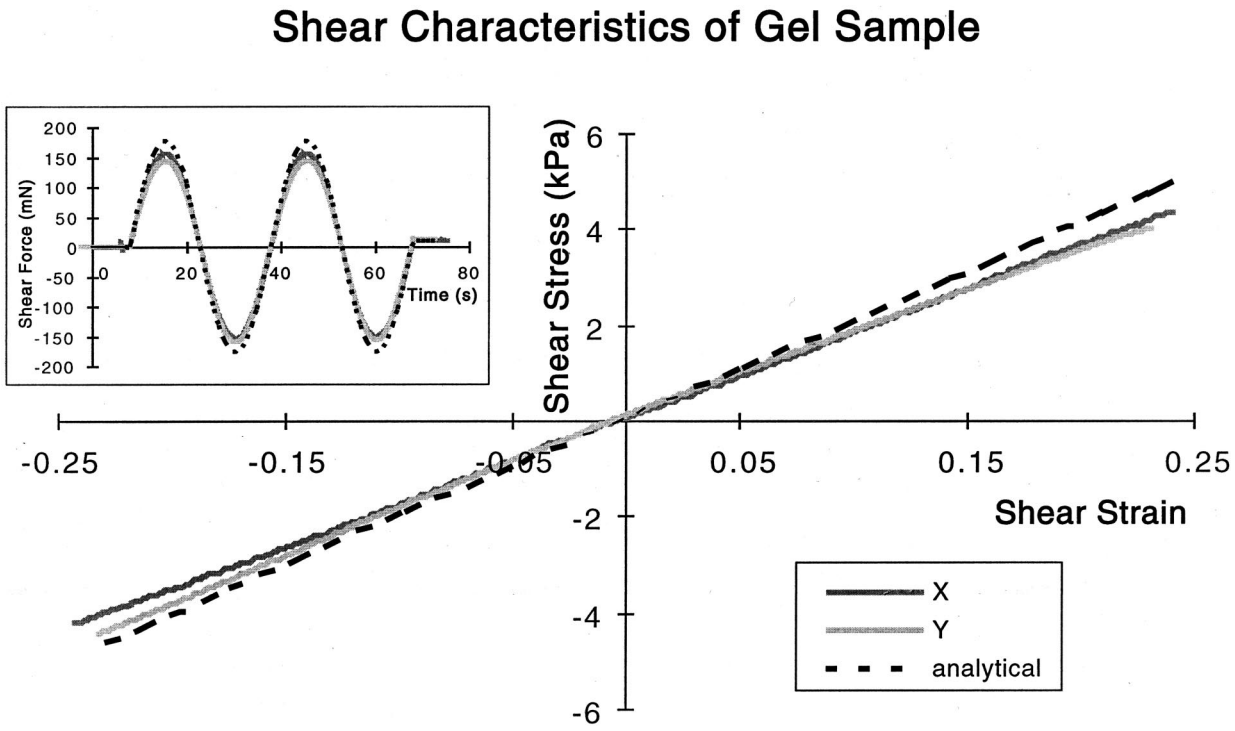

Fig. 6 Shear properties of a cuboid gel sample from batch 1 measured using the shear test device. Sinusoidal shear strains of 0.25 magnitude, 30 s period were applied over two cycles in the *X* and *Y* directions separately, as shown in the inset. The sample was not compressed in the vertical *Z* direction. Plots of corresponding shear force against shear strain are shown in the main graph. Analytical plots using a neo-Hookean material parameter of $C_1 = 10.2$ kPa obtained from the rotational shear test (see Table 1) are also superimposed on the graphs.

Table 1 Results of neo-Hookean material parameter estimation obtained from least-squares fits to each material test from 2 batches of gel. Tensile data, rotational shear data, and simple shear data for each batch were fitted to appendix Eqs. (6), (13), and (3), respectively.

Fitted Data	C_1 (±SE) kPa	
	Batch 1	Batch 2
Tensile Test	11.27 ± 0.06	13.31 ± 0.14
Rotational Shear Test	10.20 ± 0.03	12.47 ± 0.08
Simple Shear Test (from Device)	8.99 ± 0.01	11.09 ± 0.01

tively, with the apex–base direction aligned with the X axis of the device. Sinusoidal time-varying shear displacements of amplitude 1.1 mm (i.e., shear strain 0.5) and period 30 s, were applied for four cycles or more, with simultaneous measurement of shear and compressive forces. Shear displacement was applied separately along X and Y axes, corresponding to the apex–base and anterior–posterior directions, respectively. It was found that only two cycles were required to precondition the sample, after which repetitive patterns of force were obtained. Typical results for both shear and compressive stresses following preconditioning are shown in Fig. 7. A second sample was also tested from a different animal using the same protocols, with results in both X and Y directions very similar to that shown in Fig. 7. All results were reproducible across many tests on the same sample performed over a period of two hours from when the tissue was first placed in the device. On completion of these tests, samples were found to be still in a flaccid state; evidence that contracture was minimal.

As shown in Fig. 7, shear characteristics of rat septal tissue are clearly anisotropic and not symmetric about the zero strain point. Stress relaxation was evident with a time constant of the order of 10 s, and accounted for the hysteresis characteristic in the plots. In other tests on rat septum (not shown), the hysteresis was markedly increased when the sample was not placed in a bathing medium, but kept dry.

Discussion

Device Validation. Validation of the shear test device using samples of synthetic gel provided a good measure of the effectiveness of the method for characterizing shear properties of tissue. The main aim of the gel experiments was not to characterize the material properties of the gel fully, but to provide a soft-tissue-like deformation over a similar range of loads to that expected in biological tissue. This gel has previously been used to model the behavior of brain tissue in head injury studies [7] and to validate measurement of material deformation using magnetic resonance tagging [12]. Material parameters of the gel, determined independently in two gel batches by tensile and rotational shear tests, were found to differ by 10 percent from each other (Table 1). For both batches, consistent variations in relative magnitude of this parameter were seen between the three different tests, suggesting that a neo-Hookean law may not provide a complete material description. If this is true, then one would expect that the simple shear deformations imposed by the device would more closely

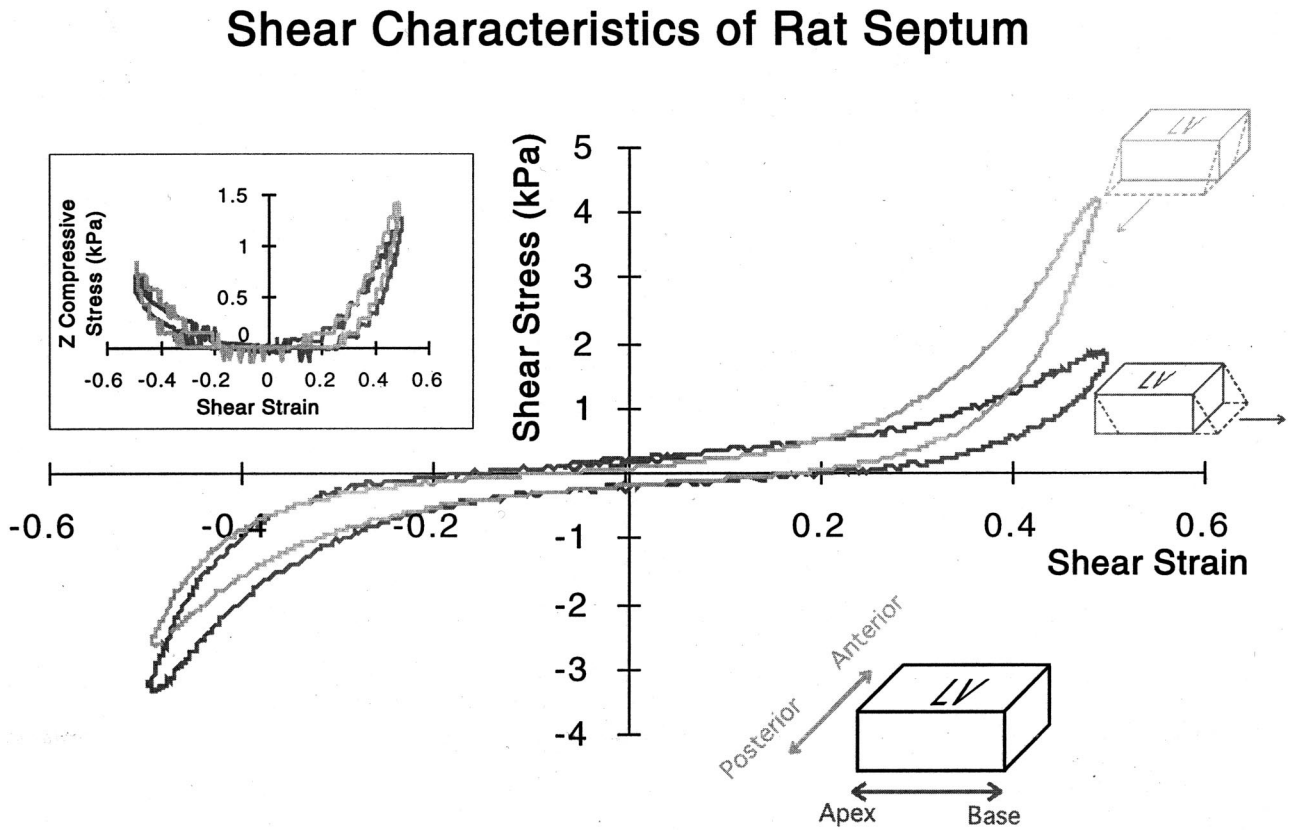

Fig. 7 Shear properties of rat septum measured using the shear test device. Sinusoidal time-varying shear displacements were applied to the RV face of a BDM-treated block of septal tissue in two orthogonal directions corresponding to the apex-base direction and the circumferential direction (anterior-posterior in intact heart). In both tests, stress-strain curves stabilized after two cycles, with stable single cycles shown in these plots. The inset graph is a plot of downward compressive force arising due to the shear strain in both directions of the sample. With the upper surface of the sample held fixed, positive base-apex strains correspond to shear displacements of the lower surface (RV side) toward the base, while positive transverse shear strains are posteriorly directed displacements.

mimic the results from the rotational shear test rather than the tensile test, as was indeed found to be the case (Table 1). It should be borne in mind, however, that such magnitudes of deviation in material parameters are routinely obtained from experiments on rubber, where material parameter estimation has been shown to depend heavily on the type of test, as well as the range of applied strain. The data of Raos, for example, show a deviation in neo-Hookean material parameter estimation of 15 percent for strains between 1.0 and 1.8 during uniaxial and biaxial tests on the same rubber compound, and even more deviation over different ranges of strains [13].

Given the inherent variation in the gel material parameter, the results from the shear-test device on the small cuboid gel sample agree remarkable well with the independent test data (Fig. 6). In this case however, an additional factor complicating the analysis is that the derivation for simple shear in the appendix makes the assumption that strains are homogeneous throughout the sample. It can readily be shown that this is not the case, as simple shear is actually impossible to achieve without the application of additional normal stresses applied unequally to the faces of the cuboid sample—the ''Poynting effect'' [11,14]. In the device no stresses are applied to the free faces of the block, hence the gel sample cannot exist in a state of homogeneous strain when deformed. Despite this qualification, the neo-Hookean material parameter obtained from the simple shear test (using homogeneous strain theory) deviated by only 15 percent from that of the independent test data. Given the low error terms in the linear calibration coefficients of the device and the clear isotropy in the X and Y directions of the sample, we were confident that the data we obtained from the device accurately reflected the shear characteristics of our gel specimen. From our results, it was clear that the device was able to measure accurately the shear characteristics of small tissue-like samples within the physiological ranges of stress and strain.

Shear Properties of Passive Myocardium. The myocardial shear data of Fig. 7 represent, to our knowledge, the first direct measurement of the shear characteristics of myocardial tissue. These experiments demonstrated the reproducibility of the apparatus over different samples and tests, as well as the ability of the device to measure nonlinearities and anisotropies in the material. As expected for a typical biosolid, the shear stress–strain characteristic was nonlinear, and exhibited hysteresis due to its viscoelastic nature [1]. The simple shear properties of septal myocardium shown in Fig. 7 are very similar in form to those observed by Talman and Boughner [6] in aortic valve cusps ($\sim$4 kPa stress at a shear strain of 1 compared with our stress of 2–4 kPa at 0.5 strain). An indirect measure of myocardial shear properties was obtained in rabbit papillary muscles using torsion experiments [15]. This tissue, which must be considered as transversely isotropic rather than orthotropic, showed similar stress–strain profiles to our mid-myocardial blocks and required a twisting moment of 0.6 mN mm for a twist of 1 rad mm^{-1}. A biaxial testing rig has also been used to investigate in-plane shear behavior of glutaraldehyde-treated bovine pericardium [16]. Again, stress–strain profiles were typical for biological materials but shear stiffness of these fixed sheets of tissue was high, reaching stresses of 40 kPa at 0.085 strain.

The anisotropic and asymmetric nature of the shear characteristics of Fig. 7 is probably due to the underlying structure of muscle fibers and cleavage planes associated with the myocardial sample in question. As septal myocardium is known to be nonuniform in muscle fiber/sheet orientation, it is difficult to characterize the contribution of its laminar and fiber structure to overall shear properties directly [17]. Nonetheless, it would be possible to use the shear test device to relate shear properties to myocardial structure if a structurally uniform sample could be obtained; possibly one excised from a larger heart than that used in this study. An alternative approach may be to use mathematical modeling techniques [18] to quantify the contribution of measured structure of the sample to its shear properties.

Device Limitations. The shear test device described in this study was designed only for quasi-static shear characterization of soft tissues. As such, maximum velocity of the DC motors used to drive the $X-Y$ translation stage was limited to 2 $mm \cdot s^{-1}$. If desired, higher rates of shear loading can be readily achieved through the use of piezoelectric actuators. A second limitation of the device was that strain measurement was confined only to external displacements of the sample surfaces. Nonhomogeneous strain fields set up within the sample could not be directly measured with the current design. In terms of constitutive law identification however, three-dimensional measurement of external strains and stresses provides sufficient quantitative information for use with a finite element modeling approach using the measured external strains and stresses as boundary constraints.

Conclusion

The shear test device for biological tissue developed in this study was capable of imposing precision bi-directional simple shear strains along with uniaxial compressive/tensile strains in the third orthogonal direction, while accurately measuring the resulting forces generated in all three axes. Simple shear characteristics of small biological samples, including anisotropic and nonlinear profiles, could be readily determined within the physiological ranges of stress and strain. Using this device, it will be possible to develop more comprehensive material descriptions of a variety of soft tissues under conditions of shear loading.

Appendix

Analytical Solutions for Gel Test Deformations. In the following derivations, we make the simplifying assumption that strains are homogeneous throughout the deformed sample. The reader is referred to Atkin and Fox [11] and Green and Zerna [19] for a more thorough analysis.

1 Simple Shear of Neo-Hookean Sample. Let particle $\mathbf{P}(X_1,X_2,X_3)$ in an undeformed neo-Hookean sample be deformed into particle $\mathbf{p}(x_1,x_2,x_3)$ by the action of simple shear applied in the X_1 direction. For this deformation, the particles move only in the X_1 direction by an amount proportional to their X_3 coordinate, described by

$$\begin{aligned} x_1 &= X_1 + KX_3 \\ x_2 &= X_2 \\ x_3 &= X_3 \end{aligned} \tag{1}$$

where K is the amount of shear in the X_1 direction. From Atkin and Fox ([11], pp. 97–98), we can write the Cauchy stress tensor as

$$\sigma = \begin{bmatrix} 2C_1K^2 & 0 & 2C_1K \\ 0 & 0 & 0 \\ 2C_1K & 0 & 0 \end{bmatrix} \tag{2}$$

where C_1 is the sole parameter describing the neo-Hookean material. On the top surface of the sample (i.e., normal to X_3), the shear stress is given by σ_{13}. Denoting the area of the top surface by A, the shear force as measured by the device is given by

$$F_{13} = 2AC_1K \tag{3}$$

2 Uniaxial Tensile Loading of Neo-Hookean Material. Let particle $\mathbf{P}(X_1,X_2,X_3)$ be deformed into particle $\mathbf{p}(x_1,x_2,x_3)$ by a uniaxial tensile load in the X_3 direction. In this case the Cauchy stress tensor ([11], p. 85) is given by

$$\sigma = \begin{bmatrix} 0 & 0 & 0 \\ 0 & 0 & 0 \\ 0 & 0 & 2C_1(\lambda^2 - \lambda^{-1}) \end{bmatrix} \tag{4}$$

where λ is the extension ratio along X_3. This represents the physical value of the stress tensor referred to the deformed cross-sectional area. Experimentally, it is more convenient to derive a measure of stress relative to the undeformed area. Thus, for an incompressible material undergoing a uniaxial stretch of λ, the cross sectional area is reduced by a factor of λ^{-1}. Relative to the *undeformed* area, the uniaxial stress component S_{33} may therefore be written as

$$S_{33} = 2C_1(\lambda - \lambda^{-2}) \tag{5}$$

with the corresponding tensile force being

$$F_{33} = 2C_1A(\lambda - \lambda^{-2}) \tag{6}$$

where A is the undeformed cross-sectional area (normal to X_3).

3 Axial Rotational Shear of a Neo-Hookean Cylindrical Tube (With Inner Surface Held Fixed). Alternative approaches to this problem are outlined in Green and Zerna [19] and Young et al. [12] in terms of cylindrical material coordinates. Let particle $P(R,\Theta,Z)$ be deformed into particle $p(r,\theta,z)$ by rotation of angle $\omega(R)$ about the z axis. This deformation may be described by

$$\begin{aligned} r &= R \\ \theta &= \Theta + \omega(R) \\ z &= Z \end{aligned} \tag{7}$$

From Green and Zerna ([19], pp. 100–101), the solutions for $\omega(R)$ and the axial couple per unit length of the tube (M) are:

$$\omega(R) = -\frac{A_1}{2C_1R^2} + A_2 \tag{8}$$

$$M = 4\pi A_1 \tag{9}$$

where A_1, A_2 are constants of integration and C_1 is the neo-Hookean material constant. The required boundary conditions on $\omega(R)$ are $\omega(a) = 0$ on the inner surface and $\omega(A) = \Phi$ on the outer surface of the tube. On solving these for A_1, A_2 we obtain

$$\omega = \frac{\Phi(a^{-2} - R^{-2})}{(a^{-2} - A^{-2})} \tag{10}$$

$$M = \frac{8\pi C_1\Phi}{a^{-2} - A^{-2}} \tag{11}$$

where a, A are the inner and outer radii, respectively. The axial couple per unit length (M) is equal to the applied couple ($2FA$) divided by the height of the tube (h), where F is the force in each arm of the couple. We can therefore rearrange Eq. (11) as

$$\Phi = \frac{A(a^{-2} - A^{-2})F}{4\pi hC_1} \tag{12}$$

and on appropriate substitution into Eq. (10) and rearranging, we obtain

$$\frac{\omega}{F} = \frac{A(a^{-2} - R^{-2})}{4\pi hC_1} \tag{13}$$

Acknowledgments

We are indebted to Professor Peter Hunter of the Department of Engineering Science, University of Auckland, for his most helpful comments and advice throughout the duration of this study. This work was funded by the Health Research Council of New Zealand.

References

[1] Fung, Y. C., 1993, *Biomechanics: Mechanical Properties of Living Tissues*, Springer-Verlag, New York.
[2] Demer, L. L., and Yin, F. C. P., 1983, ''Passive Biaxial Mechanical Properties of Isolated Canine Myocardium,'' J. Physiol. (London), **339**, pp. 615–630.
[3] Humphrey, J. D., and Yin, F. C. P., 1988, ''Biaxial Mechanical Behavior of Excised Epicardium,'' ASME J. Biomech. Eng., **110**, pp. 349–351.
[4] Smaill, B., and Hunter, P., 1991, ''Structure and Function of the Diastolic Heart: Material Properties of Passive Myocardium,'' in: *Theory of Heart*, 1st ed., Glass, L., Hunter, P., and McCulloch, A., eds., Springer-Verlag, New York, pp. 1–29.
[5] LeGrice, I. J., Takayama, Y., and Covell, J. W., 1995, ''Transverse Shear Along Myocardial Cleavage Planes Provides a Mechanism for Normal Systolic Wall Thickening,'' Circ. Res., **77**, pp. 182–193.
[6] Talman, E. A., and Boughner, D. R., 1996, ''Internal Shear Properties of Fresh Porcine Aortic Valve Cusps: Implications for Normal Valve Function,'' J. Heart Valve Dis., **5**, pp. 152–159.
[7] Margulies, S., Thibault, L., and Gennarelli, T., 1990, ''Physical Model Simulations of Brain Injury in the Primate,'' J. Biomech., **23**, pp. 823–836.
[8] Arbogast, K. B., Thibault, K. L., Pinheiro, B. S., Winey, K. I., and Margulies, S. S., 1997, ''A High-Frequency Shear Device for Testing Soft Biological Tissues,'' J. Biomech., **30**, pp. 757–759.
[9] Shuck, L. Z., and Advani, S. H., 1972, ''Rheological Response of Human Brain Tissue in Shear,'' ASME J. Basic Eng., **94**, pp. 905–911.
[10] Mulieri, L. A., Hasenfuss, G., Ittleman, F., Blanchard, E. M., and Alpert, N. R., 1989, ''Protection of Human Left Ventricular Myocardium From Cutting Injury With 2,3-Butanedione Monoxime,'' Circ. Res., **65**, pp. 1441–1444.
[11] Atkin, R. J., and Fox, N., 1980, *An Introduction to the Theory of Elasticity*, Longman, New York.
[12] Young, A. A., Axel, L., Dougherty, L., Bogen, D. K., and Parenteau, C. S., 1993, ''Validation of Tagging With MR Imaging to Estimate Material Deformation,'' Radiology, **188**, pp. 101–108.
[13] Raos, P., 1993, ''Modelling of Elastic Behavior of Rubber and Its Application in FEA,'' Plastics, Rubber Compos. Proc. Appl., **19**, pp. 293–303.
[14] Truesdell, C., 1960, *The Principles of Continuum Mechanics*, Socony Mobil Oil Company, Inc., Dallas, TX.
[15] Criscione, J. C., Lorenzen-Schmidt, I., Humphrey, J. D., and Hunter, W. C., 1999, ''Mechanical Contribution of Endocardium During Finite Extension and Torsion Experiments on Papillary Muscles,'' Ann. Biomed. Eng., **27**, pp. 123–130.
[16] Sacks, M. S., 1999, ''A Method for Planar Biaxial Mechanical Testing That Includes In-Plane Shear,'' ASME J. Biomech. Eng. **121**, pp. 551–555.
[17] LeGrice, I. J., Smaill, B. H., Chai, L. Z., Edgar, S. G., Gavin, J. B., and Hunter, P. J., 1995, ''Laminar Structure of the Heart: Ventricular Myocyte Arrangement and Connective Tissue Architecture in the Dog,'' Am. J. Physiol., **269**, pp. H571–H582.
[18] Hunter, P. J., and Smaill, B. H., 1988, ''The Analysis of Cardiac Function: a Continuum Approach,'' Prog. Biophys. Mol. Biol., **52**, pp. 101–164.
[19] Green, A. E., and Zerna, W., 1954, *Theoretical Elasticity*, Oxford University Press, Oxford.